Journal of Atmospheric and Solar-Terrestrial Physics 71 (2009) 738–743

Contents lists available at ScienceDirect

Journal of Atmospheric and Solar-Terrestrial Physics

journal homepage: www.elsevier.com/locate/jastp

Volumetric imaging of the auroral ionosphere: Initial results from PFISR ☆

Joshua Semeter [a,*], Thomas Butler [a], Craig Heinselman [b], Michael Nicolls [b], John Kelly [b], Donald Hampton [c]

[a] Department of Electrical and Computer Engineering, Boston University, 8 Saint Mary's Street, Boston, MA 02215, USA
[b] SRI International, Menlo Park, CA, USA
[c] Geophysical Institute, University of Alaska, Fairbanks, AK, USA

ARTICLE INFO

Article history:
Accepted 21 August 2008
Available online 13 September 2008

PACS:
94.20.Ac
94.80.+g

Keywords:
Incoherent scatter radar
Ionosphere
Poker Flat ISR
PFISR
AMISR
Aurora

ABSTRACT

The Poker Flat Incoherent Scatter Radar (PFISR) is the first dedicated ISR built with an electronically steerable array. This paper demonstrates the capabilities of PFISR for producing three-dimensional volumetric images of *E*-region ionization patterns produced by the aurora. The phase table was configured to cycle through 121 beam positions arranged in an 11×11 grid. A 13-baud Barker coded pulse was used, which provided ~1.5-km range resolution out to a maximum range of 250 km. Backscattered power was converted to electron density by correcting for path loss and applying the Buneman approximation assuming equal electron and ion temperatures. The results were then interpolated onto a three-dimensional cartesian grid. Volumetric images are presented at 5-min, 1-min, and 14.6-s integration times (corresponding to 960, 192, and 48 pulses-per-position, respectively) to illustrate the tradeoff between spatio-temporal resolution and data quality. At 14.6 s cadence, variability in plasma density within the volume appears to be fully resolved in space and time, a result that is supported by both observational evidence and theoretical predictions of ionospheric response times. Some potential applications of this mode for studying magnetosphere–ionosphere interactions in the auroral zone are discussed.

1. Introduction

The high-latitude ionosphere is subject to magnetospheric forcing through a variety of mechanisms (Thayer and Semeter, 2004). These sources impart a high degree of variability on the density, composition, temperature, and flows of the ionized and neutral gases. Resolving this variability in space and time is desirable for a variety of reasons. For instance, variability in the ionospheric conductance affects the rate at which Earthward poynting flux is dissipated in the neutral gas (Codrescu et al., 1995), and serves to structure electromagnetic coupling between the magnetosphere and ionosphere (Heelis and Vickrey, 1991; St. Maurice et al., 1996) possibly influencing, via feedback, the mechanism of auroral arc formation (Atkinson, 1970; Sato, 1978; Lysak, 1991). Shears in ionospheric flows mark sites of field aligned currents (Weber et al., 1991), the concomitant heating drives an outward ion flow to the magnetosphere (Tsunoda et al., 1989). Outward ion flows are also produced by soft, non-ionizing, particle fluxes (Zettergren et al., 2007), which may occur in narrow channels in the poleward regions of the auroral oval (Semeter et al., 2005).

The most comprehensive ionospheric remote sensing diagnostic is incoherent scatter radar (ISR). In the ISR technique, measurements of the backscattered power spectrum about the carrier frequency are analyzed to estimate the ion temperature (T_i), electron temperature (T_e), plasma density (N_e), and line-of-site bulk velocity (V_i) as a function of range. Information about the spatial and temporal variability in the medium is acquired by scanning the antenna. In principle, such an approach could be used to construct three-dimensional images of these parameters at some cadence. For dish antennas, such direct imaging modes have been limited to two-dimensions (e.g., range versus elevation, or range versus azimuth), owing to mechanical limitations (see Semeter et al., 2005 for an example of high-resolution two-dimensional imaging of the auroral ionization patterns using the Sondrestrom radar).

The Poker Flat ISR (PFISR) represents a new radar modality for investigating how the ionosphere responds to the rapidly varying sources of energy flux in the aurora. PFISR employs an electronically steerable array that may be re-pointed on a pulse-by-pulse basis. Direct imaging of an ionospheric volume can be achieved by acquiring range-resolved measurements over a two-dimensional array of beam positions (Nicolls and Heinselman, 2007a, b). Tradeoffs between resolution and data fidelity are controlled by

☆ This material is based upon work supported by the National Science Foundation under Grants ATM-0538868 and ATM-0547934.
* Corresponding author.
E-mail address: jls@bu.edu (J. Semeter).

1364-6826/$ - see front matter © 2008 Elsevier Ltd. All rights reserved.
doi:10.1016/j.jastp.2008.08.014

choosing pulse pattern, number and distribution of beam positions, and integration time. Because PFISR has the ability to store returns from each pulse, integration times do not have to be chosen a priori and, indeed, do not even have to be uniform over the sampled volume.

This article presents initial results from an experiment designed to image the spatiotemporal variability in the *E*-region electron density caused by auroral precipitation. To facilitate rapid formation of volumetric images, the imaged quantity is electron density estimated from range-corrected backscattered power, rather than full fitting of the computed autocorrelation function. With the current PFISR configuration, volumetric images with ~14% uncertainty may be obtained at 14.6 s cadence, which is comparable to time scales associated with *E*-region ionization. The volumetric results are compared, quantitatively, with auroral brightness measured by a collocated all-sky camera using a simple continuity calculation. The all-sky camera provides an independent measure of the ionizing source and constitutes a 'ground truth' for the ISR analysis. Limitations, tradeoffs, and future improvements are discussed.

2. Experimental description and data processing

PFISR is located at the Poker Flat Research range (65.13N, 147.47W) near Fairbanks, AK. The antenna is tilted towards the geomagnetic North so that its boresight direction corresponds to elevation 74° and azimuth 15°. The beam formed by PFISR has angular dimensions of ~1° × 1.5°, with the larger dimension in north–south plane. Geomagnetically, PFISR is located near the center of the statistical auroral oval at a magnetic L-shell of ~5. Auroras at this location are typically associated with geomagnetic storms and substorms and, hence, highly dynamic. The expected scales of spatial and temporal variability in the auroral ionization patterns must be carefully considered in designing a volumetric imaging strategy and interpreting the results. These issues are discussed quantitatively in Section 4.

For this experiment, 121 beam positions were used, arranged in an 11 × 11 grid. Fig. 1(a) shows the full set of beam positions in a horizon-based coordinate system. The beam separation was 3-degree separation in each orthogonal direction, 4.24° along the diagonal. At 100 km altitude (the nominal altitude of the ionization peak for energetic aurora) the sampled angular region subtends an approximately rectangular region with dimensions 65 km × 60 km; the horizontal spacing between the beam centers at this altitude varies from 5.2 to 6.2 km, and the beamwidth varies from ~1.7 × 2.6 to ~2.1 × 3.1 km.

Fig. 1(b) shows the beam positions superimposed on an image recorded with the collocated all-sky camera. The aurora near the horizon are artificially saturated to emphasize detail within the PFISR volume. Note that in an image of the sky from the ground, east and west directions are flipped compared with map coordinates since the ground-based perspective is a mirror of the map perspective. Both the radar and all-sky image in Fig. 1 are depicted in the native coordinate system of an all-sky image—i.e., west is clockwise from north.

PFISR has the ability to transmit and receive on multiple frequency channels near 450 MHz, allowing for multiple pulse patterns to be transmitted within the duty cycle. For this experiment, three channels were used. On one channel an uncoded 480 μs pulse was used. These returns allow for estimation of the plasma autocorrelation function (derived from lag products), from which plasma parameters may be estimated via model fitting. However, because of the long pulse length (72 km), these measurements are of limited use for studying the narrow layers associated with auroral ionization.

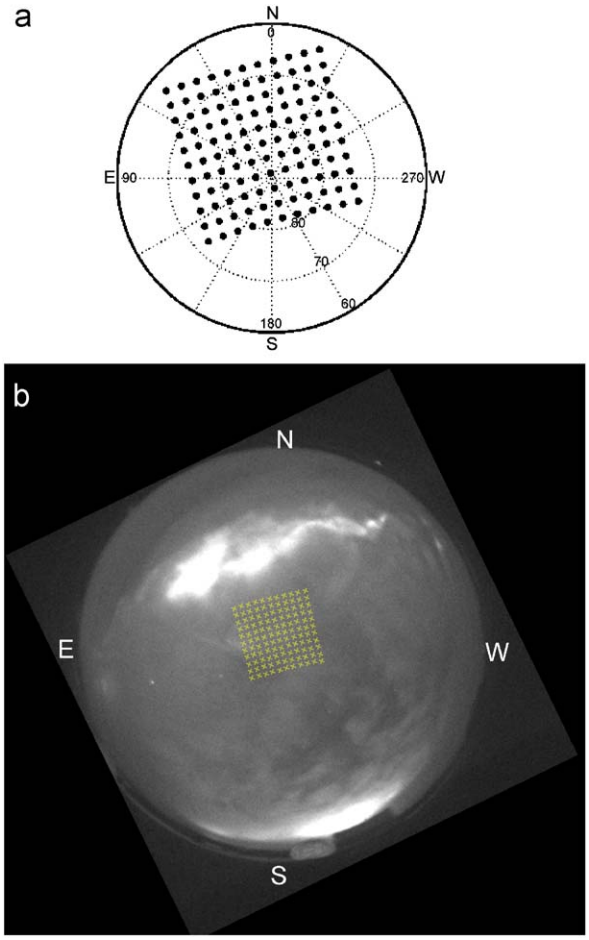

Fig. 1. (a) PFISR beam positions used in this experiment, depicted in a horizon-based polar coordinate system. (b) Beam positions superimposed on an image recorded with the collocated all-sky camera.

On the other two channels, a 13-baud Barker coded pulse was transmitted (Gray and Farley, 1973). The pattern was constructed using 10 μs bauds. After demodulation, these measurements provided estimates of backscattered power at ~1.5 km range resolution. Power was then converted to N_e using the Buneman approximation (Evans, 1969) under the assumption that the electrons and ions are thermalized ($T_e = T_i$), which results in the expression

$$N_e(z) = \frac{2C_s r^2 P_r(z)}{P_t \tau}, \quad (1)$$

where r, range to target volume determined by time delay; P_t, transmitted power; P_r, backscattered power; τ, pulse length; C_s, constant term, embodying physical and radar system constants.

The $T_e = T_i$ assumption is generally valid in the collision-dominated *E*-region (see, e.g., Semeter and Kamalabadi, 2005) but may be violated within the auroral electrojet (near 110 km) as a consequence of anomalous heating associated with the Farley–Buneman (F–B) instability (Schlegel and St. Maurice, 1981). The instability would cause a reduction in backscattered power and an underestimation of N_e from Eq. (1). However, the F–B instability requires electric fields exceeding ~50 mV/m. Such fields are not generally found within regions of auroral ionization (de la Beaujardiere et al., 1977; Marklund, 1984) owing to the high electrical conductivity within the arc regions. Although the lack of knowledge of plasma temperatures is a clear limitation of this mode, it is likely that Eq. (1) is valid within the auroral structures we are observing.

The full grid of 121 positions was sampled at each frequency every 0.61 s. To reduce the amount of data, returns from 24 pulses were averaged prior to storing. This number was chosen based on considerations of data fidelity. For the high SNR expected in these measurements, uncertainties vary approximately as $1/\sqrt{K}$, where K is the number of independent samples (Farley, 1969). Averaging the two Barker-coded channels over 24 pulses gives an uncertainty of $1/\sqrt{48}\sim14.4\%$. This was deemed the maximum acceptable uncertainty in our estimates of N_e. The finest temporal resolution at which volumetric images may be constructed is thus $24\times0.61=14.6$ s.

The radar observations were supported by a collocated all-sky white-light camera. The camera was configured to record images at 10 s cadence at an exposure time of 0.25 s. The all-sky camera observations provided invaluable context for interpreting the PFISR volumetric images, as discussed in the next section.

3. Results

The results presented here are from an experiment conducted on November 10, 2007, between 0800 and 1300 UT (2300–0400 Local Time). Although the weather was partly cloudy, the all-sky images showed evidence for moderate auroral activity throughout this period, with the aurora occasionally intersecting the volume sampled by PFISR. To visualize the volumetric measurements, the N_e were interpolated onto a regular three-dimensional cartesian grid using tri-linear interpolation. We begin with a representative example showing how radar and optical measurements may be jointly analyzed to simultaneously study the magnetospheric forcing and the ionospheric response to an auroral event. We then proceed to demonstrate the capabilities of the volumetric mode for studying time variations in ionospheric structure.

3.1. Radar–optical comparison

Fig. 2 presents an example of a three-dimensional volumetric image corresponding to a period of auroral activity within the PFISR volume. The volumetric data are represented by three horizontal cuts (100, 107, and 120 km) and one vertical cut, aligned with an approximate magnetic meridian a few kilometers east of the radar. The densities were computed from 1-min averages of P_r (= 192 pulses per position, RMS uncertainty of ~7%). The figure depicts an E-W auroral ionization structure. Electron densities are seen to exceed 10^{12} m^{-3} down to 100 km altitude, indicating the presence of primary electron energies in the ~20 keV range (e.g., Semeter and Kamalabadi, 2005, Fig. 3).

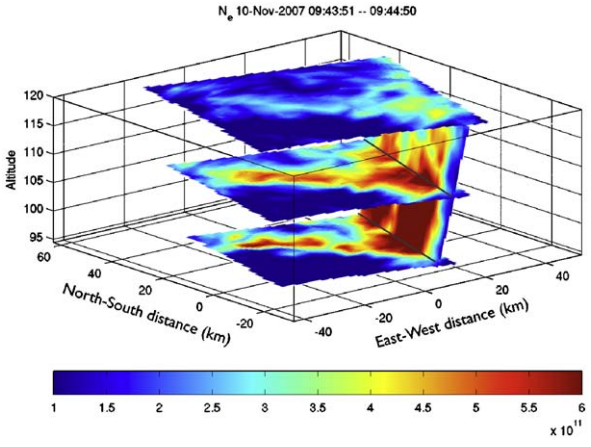

Fig. 2. Volumetric image of *E*-region on 10 November 2007, 09:43:51–09:44:50 UT. The image was produced by averaging 192 pulses-per-position. The horizontal cuts are at 100, 107, and 120 km. The structured density enhancement seen in the image was produced by auroral electron precipitation in the ~20 keV range.

Fig. 3a shows the corresponding auroral image averaged over the PFISR integration window. The figure is a cropped version of the all-sky image used in Fig. 1(b). Again, image quality is degraded due to overcast weather conditions, but the auroral features are nonetheless visible. Examination of the full-cadence all-sky images showed that the aurora was not particularly active during this interval, and the 1 min integration time used in Fig. 2 should provide a reasonable representation of the *E*-region structure associated with these optical features.

A quantitative comparison of optical and radar measurements may be made by noting that plasma density and photon production are related through a continuity equation. In the collision dominated *E*-region, continuity is approximated as a steady-state balance between plasma production and loss ($P=L$). For energetic electron precipitation (i.e., characteristic energy >5 keV), the dominant emissions in the pass-band of a white-light Silicon-based CCD camera are the oxygen 557.7 nm line, the N_2 first positive group bands, the N_2 first negative group bands, and the N_2^+ Meinel bands (Chamberlain, 1961; Rees and Luckey, 1974; Strickland et al., 1989), with the aggregate brightness roughly proportional to the rate of ion production, q, integrated along the line of sight (Semeter and Doe, 2002). On the other side of the continuity equation, plasma is lost via chemical recombination at a rate given by $\alpha N_i N_e=\alpha N^2$, where $N=N_e=N_i$ (quasi-neutral assumption) and α is the altitude-dependent recombination coefficient. Under these assumption, the continuity equation is expressed by $q=\alpha N^2$. The range of validity of this expression is discussed by Semeter and Kamalabadi (2005). In the auroral zone the approximation is valid for altitudes <150 km, and for auroral sources that vary with time scales greater than a few seconds.

To apply this model, note that both the camera and the radar observe in the same polar coordinate system, such that a given PFISR beam position corresponds to a group of pixels in the all-sky images. The precise set of pixels is determined by the angular dimensions of the radar beam. To within a constant, an estimate of optical brightness ε is obtained by integrating αN^2 over range, i.e.,

$$\hat{\varepsilon}\sim\int_0^\infty \alpha N^2\,dr. \tag{2}$$

Fig. 3(b) shows contours of $\hat{\varepsilon}$ superimposed on the auroral image of panel a. For this calculation, we used the empirical expression for α given by Vickrey et al. (1982) ($\alpha=2.5\times10^{-12}e^{-z/51.2}$ m^3/s, where z is geographic altitude in kilometers). The positions of the auroral features and their relative intensities are well represented by the contours. This simple technique provides a means of evaluating models of ionospheric continuity within regions of auroral production. For more dynamic auroras or different electron energy ranges, these estimates are not expected to agree as well as discussed in Section 4.

3.2. Time-dependent results: 5-min samples

One of the strengths of this technique is the ability to resolve the three-dimensional response of the ionosphere to an auroral event as a function of time. Magnetospheric disturbances may produce ionospheric variability over time scales of seconds (dynamic aurora), minutes (pulsating aurora), hours (substorm), or days (main phase storm). As stated in the Introduction, the PFISR data acquisition architecture is flexible, and it is not

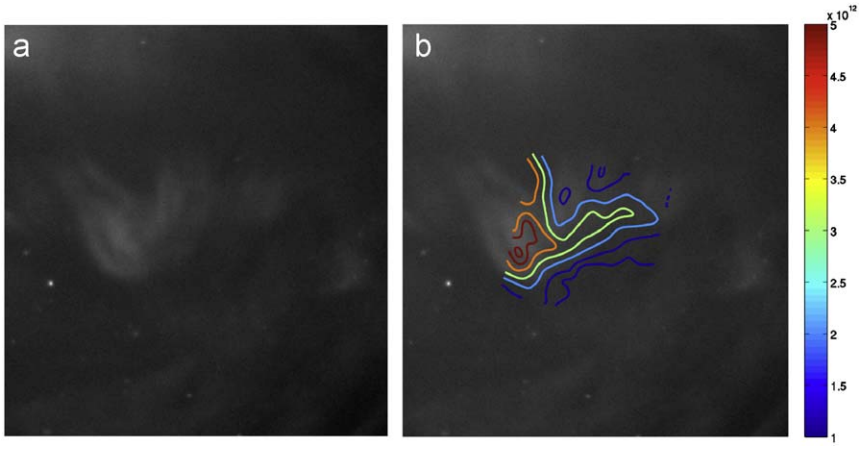

Fig. 3. (a) An average auroral image corresponding to the period shown in Fig. 2. The image is a cropped version of the all-sky image shown in Fig. 1(b). (b) Same image overlain with contours of $\int \alpha N_e^2 \, dr$, computed from PFISR measurements.

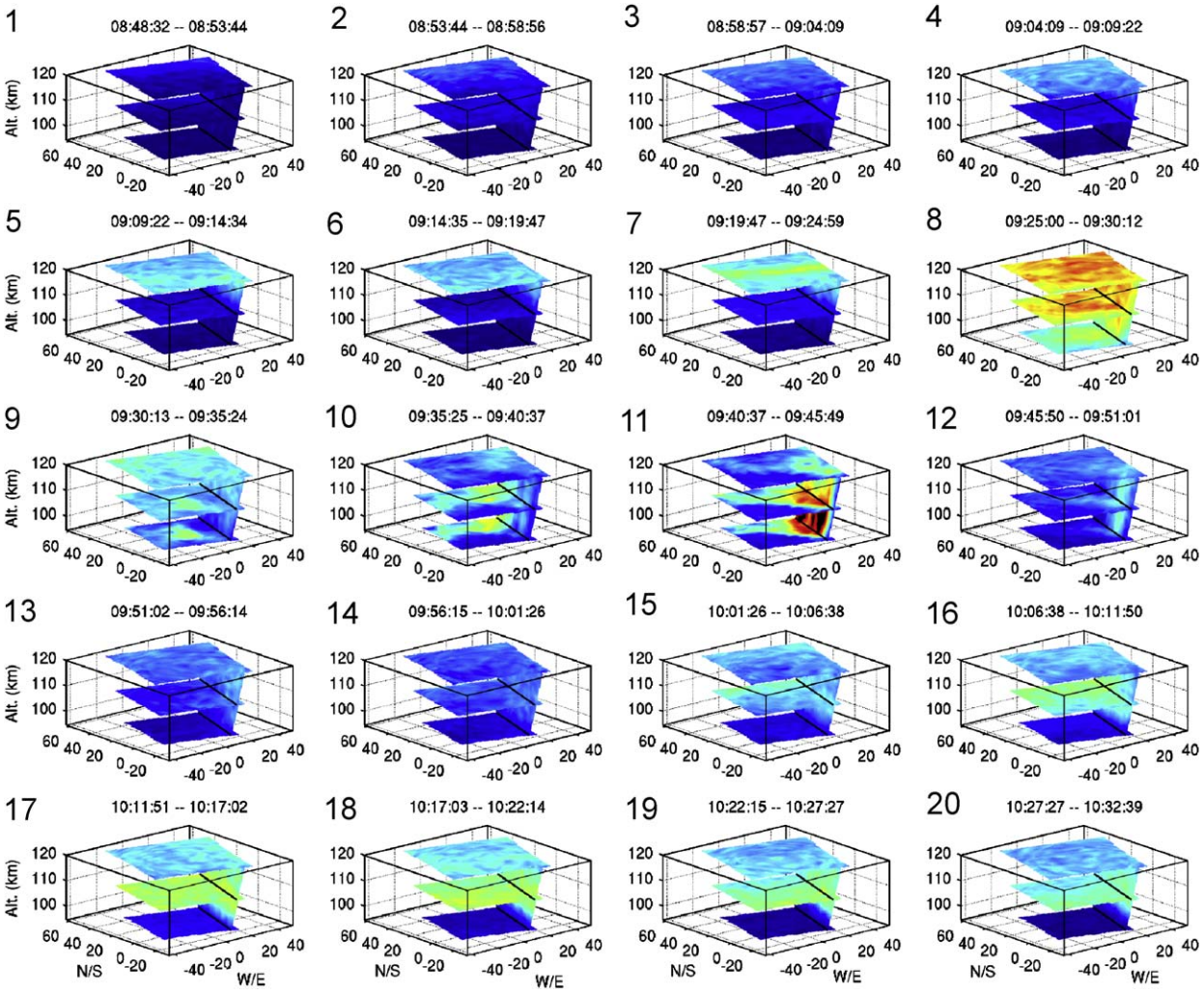

Fig. 4. PFISR volumetric images constructed with 5-min integration (960 pulses-per-position) covering a 100-min period (same color scale as Fig. 2).

necessary to determine a priori which of these physical time scales is to be targeted. In this section and the next, we highlight two different scales of variability observable in our data.

Fig. 4 presents a summary of contiguous PFISR images recorded with 5-min integration (960 pulses per beam position) covering an interval of ~100 min. The interval begins with a uniform low-density *E*-region (panel 1). Panels 1–8 document a monotonic increase in density in the 120-km cut (corresponding to primary electron energies of ~2 keV). The rate of increase is not constant however; the largest jump occurs from panels 7 to 8.

Moreover, at this resolution, the density increase appears to occur simultaneously over a large horizontal region.

After panel 8, the density at 120 km decays, and a more structured density enhancement grows in the 100 and 107-km cuts (panel 11). Auroral ionization below 100 km is associated with primary electron energies above 20 keV. After panel 11 this structure abates, and the ionization appears primarily in the 107 km cut. An ionization peak at this altitude corresponds to primary auroral electron with energy 10 keV.

3.3. Time-dependent results: 14.6-s samples

The ionospheric response to an individual arc activation cannot be resolved at five-minute resolution. For this, we turn to volumetric images produced at the maximum available frame rate ($1/14.6 = 0.07$ Frames/s). Fig. 5 shows a contiguous sequence of such images over the 2-min interval preceding the interval of panel 8 in Fig. 4. The image quality is still quite reasonable even at this cadence. Here we see the development of an auroral ionization structure in the 120 km cut. Examination of the vertical slice shows that the ionization extended down to nearly 107 km. Of note is the fact that this structure is also observed in at least three sequential images in roughly the same location. This suggests that we are fully resolving this event in time at this cadence.

Figs. 6 and 7 present two more examples at this resolution, illustrating other morphologies observed in our data. The all-sky camera observations suggest that these structures may be associated with pulsating auroral patches. In Fig. 6, an annular density enhancement is seen to form in the 100 km cut. Again, the appearance of this structure in multiple frames suggests that the time variability is fully resolved at this cadence. Fig. 7 shows an example of a density structure which has an apparent motion from east to west through the field-of-view. Since recombination times are of order a few seconds at these altitudes, the apparent motion is actually caused by motion of the ionizing source.

4. Discussion and conclusions

We have performed an initial evaluation of the capabilities of the PFISR for producing three-dimensional volumetric images of aurorally induced structure in the ionospheric *E*-region. The volumetric images were constructed from measurements of range-corrected power recorded at 121 beam positions arranged in an 11×11 grid. With this mode, volumetric images with ~14% uncertainty can be formed at 14.6-s cadence. Although this period is certainly long compared with the fastest time scales of auroral variability (e.g., Semeter and Blixt, 2006), it is similar to the *E*-region response time. Specifically, an effective time constant governing the plasma density response is $\tau = 1/\alpha N^2$. Semeter and Kamalabadi (2005) showed how this time constant is expected to vary over altitude and density space. Typical ranges for energetic auroral precipitation are 100–130 km in altitude and 10^{11}–10^{12} m^{-3} in density. These ranges correspond to time constants between 2 and 20 s. Thus, the rapid variability observed in the optical signal is 'filtered out' in the ionospheric response. The mode described herein is suitable for most conditions. This conclusion was demonstrated in the context of Figs. 5–7,

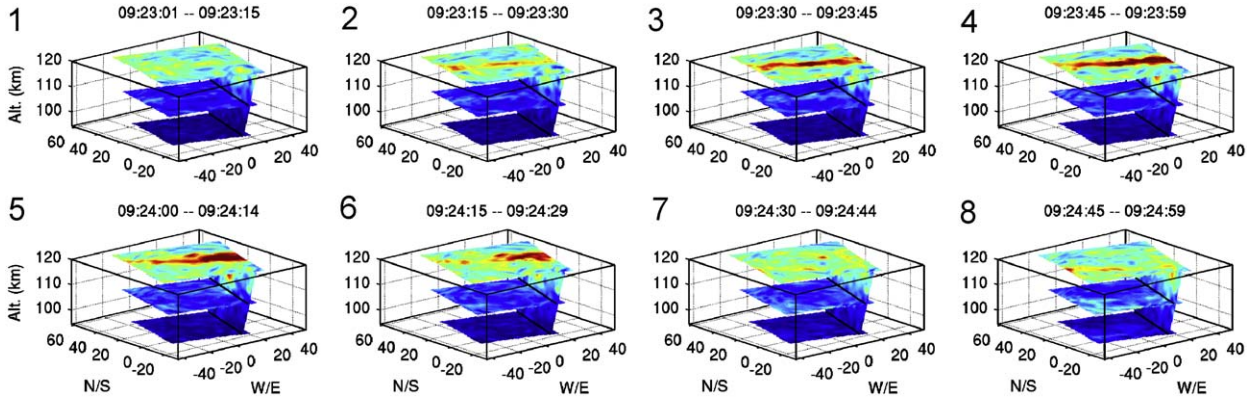

Fig. 5. PFISR volumetric images at 14.6-s cadence in the interval 09:23:01–09:24:59 UT, showing the formation and decay of an east–west arc-related ionization enhancement at ~120-km (same color scale as Fig. 2).

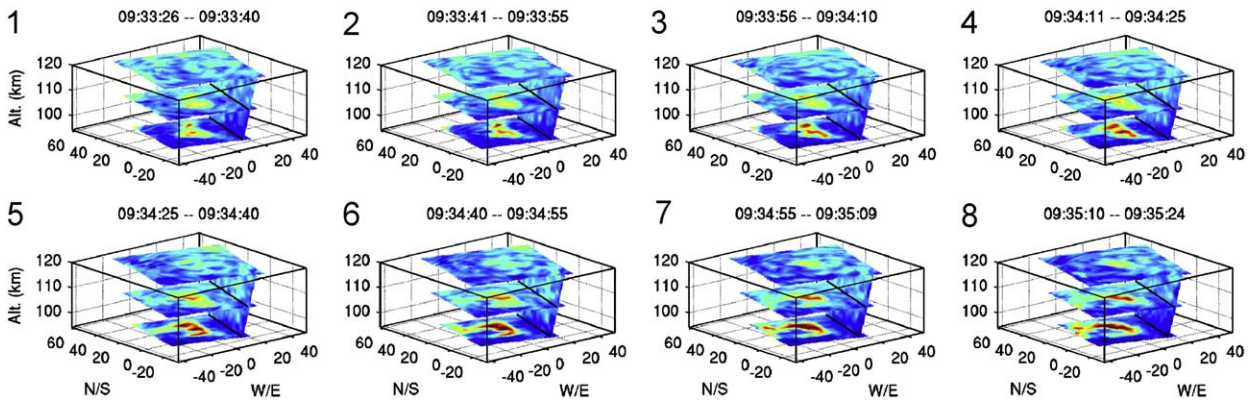

Fig. 6. Another interval at 14.6-s cadence (09:33:26–09:35:24 UT), showing the formation of an annular plasma enhancement at ~100 km (same color scale as Fig. 2).

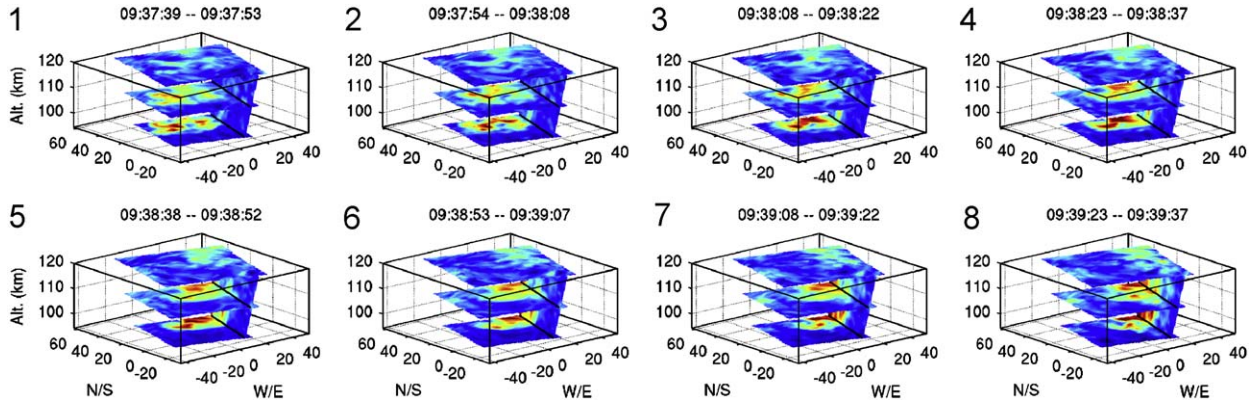

Fig. 7. Another interval at 14.6-s cadence (09:37:39–09:39:37 UT), showing a structure 'moving' from west to east in successive frames at ~100-km (same color scale as Fig. 2).

which suggest that density variations were essentially fully resolved in time.

The availability of simultaneous measurements by a collocated imaging system suggest many research possibilities. One possibility is the experimental determination of the *E*-region time constant (hence, recombination rate). Although the conditions for this experiment were somewhat overcast, we have shown good agreement between optical luminosity and radar estimates of line-of-sight integrated energy deposition rate for a slowly varying aurora. A careful analysis of time-dependent measurements during more dynamic conditions will allow us to evaluate time-dependent continuity.

The radar-optical comparison in Fig. 3 would also disagree if the causative particle spectrum was soft, such that emissions associated with non-ionizing collisions (such as OI 630 nm) become an important contributor to the aggregate white light luminosity. In such situations, a more comprehensive model connecting radar and optical measurements is needed. For instance, using fitted ISR spectra, one could produce volumetric images of T_e and T_i as well as N. With these measurements, most of the auroral spectrum can be estimated (Zettergren et al., 2007), testing our understanding of the time-dependent response of the ionosphere to auroral inputs.

In summary, the experiment described herein demonstrates that three-dimensional images of the ionospheric response to auroral forcing can be obtained at a meaningful resolution and cadence using the PFISR facility. This capability opens up many new possibilities for studying magnetosphere–ionosphere interactions. The approach is further enhanced when coordinated measurements by independent sensors are available, such as auroral imagery or ground-based magnetometry.

References

Atkinson, G., 1970. Auroral arcs: result of the interaction of a dynamic magnetosphere with the ionosphere. Journal of Geophysics Research 75 (25), 4746–4754.

Chamberlain, J.W., 1961. Physics of the Aurora and Airglow. Academic Press, New York.

Codrescu, M.V., Fuller-Rowell, T.J., Foster, J.C., 1995. On the importance of E-field variability for Joule heating in the high-latitude thermosphere. Geophysics Research Letters 22 (17), 2393–2396.

de la Beaujardiere, O., Vondrak, R., Baron, M., 1977. Radar observations of electric fields and currents associated with auroral arcs. Journal of Geophysics Research 82, 5051.

Evans, J., 1969. Theory and practice of ionospheric study by Thomson scatter radar. Proceedings of the IEEE 57, 496–530.

Farley, D.T., 1969. Incoherent scatter correlation function measurements. Radiation Science 4, 935–953.

Gray, R., Farley, D., 1973. Theory of incoherent-scatter measurements using compressed pulses. Radiation Science 8 (2), 123–131.

Heelis, R.A., Vickrey, J.F., 1991. Energy dissipation in structured electrodynamic environments. Journal of Geophysics Research 96, 14189.

Lysak, R.L., 1991. Feedback instability of the ionospheric resonant cavity. Journal of Geophysics Research 96, 1553–1568.

Marklund, G.T., 1984. Auroral arc classification scheme based on the observed arc-associated electric field pattern. Planetary Space Science 32 (2), 193–211.

Nicolls, M., Heinselman, C., 2007a. Imaging of polar mesosphere summer echoes with the 450 MHz Poker Flat Advanced Modular Incoherent Scatter Radar. Geophysics Research Letters, L20102.

Nicolls, M., Heinselman, C., 2007b. Three-dimensional measurements of traveling ionospheric disturbances with the Poker Flat Incoherent Scatter Radar. Geophysics Research Letters, L21104.

Rees, M., Luckey, D., 1974. Auroral electron energy derived from ratio of spectroscopic emissions, 1, model computations. Journal of Geophysics Research 79, 5181–5186.

Sato, T., 1978. A theory of quiet auroral arcs. Journal of Geophysics Research 83, 1042–1048.

Schlegel, K., St. Maurice, J.-P., 1981. Anomalous heating of the polar E region by unstable plasma waves. I. Observations. Journal of Geophysics Research 86 (1447–1452), 1042–1048.

Semeter, J., Blixt, E., 2006. Evidence for alfvén wave dispersion identified in high-resolution auroral imagery. Geophysics Research Letters 22, L13106.

Semeter, J., Doe, R., 2002. On the proper interpretation of ionospheric conductance estimated through satellite photometry. Journal of Geophysics Research 107 (A8).

Semeter, J., Kamalabadi, F., 2005. Determination of primary electron spectra from incoherent scatter radar measurements of the auroral *E*-region. Radiation Science 40, RS2006.

Semeter, J., Heinselman, C., Sivjee, G., Frey, H., Bonnell, J., 2005. Ionospheric response to wave accelerated electrons at the poleward auroral boundary. Journal of Geophysics Research Letters 110 (A9), 11310.

St. Maurice, J.-P., Kofman, W., James, D., 1996. In situ generation of intense parallel electric fields in the lower ionosphere. Journal of Geophysics Research 101, 335–356.

Strickland, D., Meier, R., Hecht, J., Christensen, A., 1989. Deducing composition and incident electron spectra from ground-based auroral optical measurements: theory and results. Journal of Geophysics Research 94 (A10), 13,527–13,539.

Thayer, J., Semeter, J., 2004. The convergence of magnetospheric energy flux in the polar atmosphere. Journal of Atmospheric Solar-Terrestrial Physics 66, 805–817.

Tsunoda, R.T., Livingston, R.C., Vickrey, J.F., Heelis, R.A., Hanson, W.B., 1989. Dayside observations of thermal-ion upwellings at 800-km altitude—an ionospheric signature of the cleft ion fountain. Journal of Geophysics Research 94 (13), 15277–15290.

Vickrey, J., Vondrack, R., Matthews, S., 1982. Energy deposition by precipitating particles and joule dissipation in the auroral ionosphere. Journal of Geophysics Research 87 (A7), 5184–5196.

Weber, E., Vickrey, J., Gallagher, H., Weiss, L., Heinselman, C., Heelis, R., Kelly, M., 1991. Coordinated radar and optical measurements of stable auroral arcs on the polar cap boundary. Journal of Geophysics Research 96 (A10), 17,847–17,863.

Zettergren, M., Semeter, J., Blelly, P.-L., Diaz, M., 2007. Optical estimation of auroral ion upflow: Theory. Journal of Geophysical Research 112, A12310, doi:10.1029/2007JA012691.